DNS of Low Reynolds Number Flow Dynamics of a Thin Airfoil with an Actuated Leading Edge

Final Report by

Sourabh V. Apte

School of Mechanical Industrial Manufacturing Engineering

Oregon State University

ASEE Summer Faculty Fellowship Program

Wright-Patterson Airforce Base

June 27-August 27 2010

AFRL Research Advisor and Sponsor: Dr. Miguel Visbal

Acknowledgement

Abstract

Use of oscillatory actuation of the leading edge of a thin, flat, rigid airfoil, as a potential mechanism for control or improved performance of a micro-air vehicle (MAV), was investigated by performing direct numerical simulations at low Reynolds numbers. The leading edge of the airfoil is hinged at one-third chord length allowing dynamic variations in the effective angle of attack through specified oscillations (flapping). This leading edge actuation results in transient variations in the effective camber and angle of attack that can be used to alleviate the strength of the leading edge vortex at high angles of attack. A fictitious-domain based finite volume approach [Apte et al., JCP 2009] was used to compute the moving boundary problem on a fixed background mesh. The flow solver is three-dimensional, parallel, second-order accurate, capable of using structured or arbitrarily shaped unstructured meshes and has been validated for a range of canonical test cases including flow over cylinder and sphere at different Reynolds numbers, and flow-induced by inline oscillation of a cylinder. Flow over a plunging SD7003 airfoil at two Reynolds numbers (1000 and 10,000) was computed and results compared with those obtained using AFRL's high-fidelity solver [Visbal, AIAA J. (2009)] to show good predictive capability.

To assess the effect of an actuated leading edge on the flow field and aerodynamic loads, two-dimensional parametric studies were performed on a thin, flat airfoil at 20 degrees angle of attack and Reynolds number of 14,700 (based on the chord length) with sinusoidal actuation of the leading edge over a range of reduced frequencies (k=0.57-11.4) and actuation amplitudes. It was found that high-frequency, low-amplitude actuation of the leading edge significantly alters the leading edge boundary-layer and vortex shedding and increases the mean lift-to-drag ratio. This study indicates that the concept of an actuated leading-edge has potential for development of control techniques to stabilize and maneuver MAVs in response to unsteady perturbations at low Reynolds numbers.

The summer research at AFRL's computational sciences division has resulted in several opportunities for future collaborations with AFRL scientists and researchers. At Oregon State, new projects for senior students are initiated to build and modify the existing physical setup and measure lift and drag coefficients.

1 Introduction and Objectives

The desire to advance the use of thin, low Re wings at small scales introduces flow dynamics that significantly influence their performance and flow control. At sufficiently high angles of attack during transients, flow over an airfoil separates, which can lead to a 'dynamic stall' condition. One major concern of thin airfoil design, when operating at high lift conditions, is the unsteady nature of separation at the leading edge resulting in a Kelvin-Helmhotlz type flow instability [1, 2, 3]. This causes the generation and convection of low frequency large vortical structures that have a strong influence on unsteady lift. Very early works on flow over hydrofoils and wings [4, 5] have shown a strong correlation of pressure in the separation bubble with the onset of stall conditions.

For **very low Reynolds number** [$\mathcal{O}(100)$], the unsteady flow characteristics of thin wings undergoing plunge maneuvers show downstream advection of the leading edge vortex and the frequency for unsteady lift characteristics [6]. Other studies of unsteady flow characteristics during pitching include [7, 8, 9, 10] and recent computational work based on immersed boundary technique under the AFOSR MURI program at CalTech on impulsively started wing [11, 12, 13]. It is clear from these and other studies that vortex shedding, advection, and strength is highly dependent on the maneuvering characteristics.

Extensive studies at low Re have been carried out to better understand the flow and its dynamic characteristics for stability and control considerations. At low Re, thin flat airfoils actually *delay* stall to higher angles of attack when operating at lower aspect ratios, although the lift is somewhat lower at lower angles of attack [14]. It has been shown that a cambered plate (4%) performs better in the Re range of 10^4–10^5 [14], and has a low sensitivity to the trailing edge geometry and the turbulence intensities [15]. Although thin airfoils show many advantages at low Re, such as high lift-to-drag ratio, they exhibit *wide fluctuations in lift* mainly caused by the unsteady flow separation at the leading edge ([16] and references therein). The character of this separation is highly unsteady, at fairly low frequencies, and generally without reattachment if the angle of attack is sufficiently large [16], however, most of this work is at somewhat higher Re ($\sim 3 \times 10^5$). As the angle of attack is increased to the stall condition there is a rise in the unsteady character of the lift coefficient, with rms fluctuations on the order of 0.1–0.2. This is in contrast to the unsteady lift coefficients which are on the order of 0.03 for trailing edge stall. The thin airfoil stall versus angle of attack is associated with a drop in lift coefficient, a rise in unsteadiness and then a subsequent rise in lift, and it is asserted that the unsteadiness in lift is a direct consequence of the leading edge separation [16]. Effect of impressed acoustic excitation of the airfoil as a method of flow control [17] has been investigated to reduce the unsteadiness in flow separation and lift oscillations. Vorticity mapping, to quantify unsteady flow associated with airfoil motion, has been used to correlate thrust with shedding frequency [18].

Leading Edge Actuation:

The primary objective of the proposed work is to investigate, using direct numerical simulations the potential benefits to the lift and drag characteristics of an oscillating leading edge on thin, flat airfoils at low Reynolds numbers $[\mathcal{O}(10^4)]$ with and without pitching maneuvers (see Figure 1). The **central hypotheses** driving the proposed research are: (i) Oscillatory actuation of the leading edge provides an effective mechanism to control transients in lift, drag, and pitching moment during steady and transient flow conditions at low Reynolds numbers $[\mathcal{O}(10^4)]$ by reducing the strength of the generated vortex and weakening the separation bubble; (ii) Actuation time scales and waveforms associated with the flap motion can *positively* influence the lift characteristics by altering the leading-edge vortex shedding, separation-bubble dynamics, and dynamic stall conditions.

Figure 1: Schematic of a thin, flat airfoil with a leading edge actuator. A typical flap, length (ℓ_f) approximately 30% of the chord (c), will be hinged to the airfoil body to facilitate change in flap angles (θ). The angle of attack (α) will also be changed representative of pitching maneuvers.

The chief **aim** is to parameterize the flow field and vortex dynamics over a range of angles of attack and flap angle for a fixed flap-length to chord ratio at low Reynolds numbers under steady and unsteady flow conditions representative of an airfoil undergoing characteristic maneuvers. New insights into the flow dynamics can then be used to develop a reduced-order models for active control of the lift-to-drag ratio. The following **research tasks** are identified to test the defined hypotheses:

I. Verification of the Fictitious Domain Approach for Flapping Leading Edge: First, the fictitious domain method developed by Apte *et al.* [19] is used to compute flow over a plunging SD7003 airfoil, commonly used for study of MAVs. Results for low Re (1000 and 10000) is verified against AFRL's high-fidelity FDL3DI solver [20, 21]. A grid-refinement study is also performed to identify resolution requirements necessary to capture important flow features.

II. Quantify the effect of dynamic changes in angles of attack relative to flap angle on the lift and drag: Effect of sinusoidal variations in the angle of attack ($\dot{\alpha}$) actator angles ($\dot{\theta}$) at a fixed angle of attack ($\alpha = 20°$) on the lift and drag coefficients is investigated for a wide range of oscillation frequencies (1, 3, 5, 10, and 20 Hz) and actuation amplitudes ($\Delta\theta = 2.5°, 5°, 10°$). Effect of the actuation on the mean lift-to-drag ratio is computed and compared with the no-actuation case.

2   Methodology:
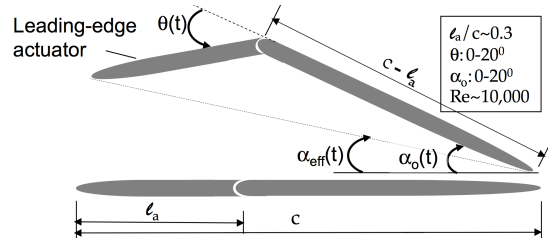
The computational algorithm for flow over immersed objects on simple Cartesian grids is based on a fictitious domain approach [22, 19, 23]. In this approach, the entire fluid-rigid body domain is assumed to be an incompressible, but variable density, fluid. The flow inside the fluid region is constrained to be divergence-free for an incompressible fluid, whereas the flow inside the particle (or rigid body) domain is constrained to undergo rigid body motion (i.e. involving translation and rotational motions only). For specified motion of the rigid body, the rigidity constraint force can be readily obtained once the location of the boundary of the rigid body is identified by making use of marker points in a banded region surrounding the rigid body surface (figure 2).

The marker points provide subgrid scale resolution, improving the accuracy of interpolations between the marker points and the background grid. Due to rigidity of the moving object, there is no relative motion between the marker points, and all points move with the same, specified velocity field. The rigidity constaint force is then enforced explicitly in a standard fractional step scheme. The flow solver is fully parallel and based on conservative finite volume scheme [25] for accurate prediction of turbulent flows and has been verified on a variety of canonical test cases such as flow over a cylinder, sphere and a NACA airfoil to show good predictive capability.
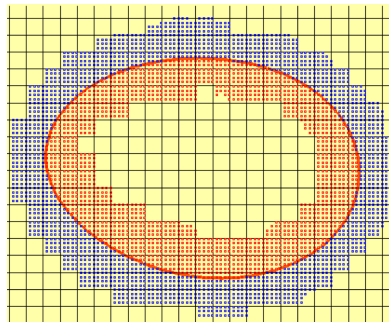

Figure 2: Use of banded marker points to identify the rigid body surface in a fictitious-domain approach [24, 19].

3   Results:

Computational studies involving verification tests on a SD7003 plunging airfoil and parametric studies of leading edge actuation for a thin, flat airfoil are presented below.

3.1   Verification Tests

The fictitious-domain approach was used to simulate flow over a plunging SD7003 airfoil, corresponding to the high-fildeity simulations by Visbal [20, 21]. This configuration has also been a subject of several experimental and numerical studies [26]. The case with chord Reynolds numbers of 10^3 and 10^4 were used to assess the predictive capability of the present solver. This airfoil has a maximum thickness of 8.5% and

Grid	$\Delta x/c$	$\Delta y/c$
Baseline	0.00275	0.00275
Coarse	0.005	0.005
Non-Uniform	0.005	0.0008
$\Delta t U_\infty/c$	0.0002	CFL$\sim$ 0.2

Figure 3: Cartesian grid resolution for plunging SD7003 cases.

a maximum camber of 1.45% at 35% chord length. The original sharp trailing edge was rounded with a circular arc of radius ($r/c \approx 0.0004$, c is the chord length) corresponding to the simulations by Visbal [20].

3

The grid resolution and time-step used for this study are given in figure 3. A simple Cartesian grid refined in a small patch around the airfoil was used. Two grid points were used in the spanwise direction, with periodic conditions, for this two-dimensional study. Visbal [21] used a body-fitted, moving grid, sixth-order accurate algorithm with wall-normal resolution of 0.00005 and 0.0001 for baseline and coarse grids, respectively. The corresponding resolutions along the airfoil surface were 0.005 and 0.01, respectively.
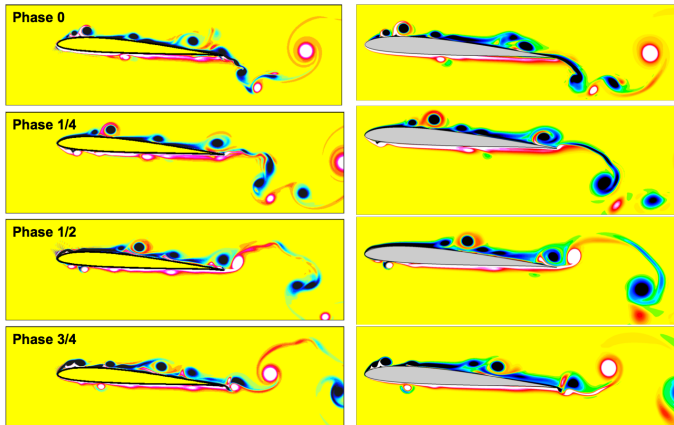

Figure 4: Instantaneous, out-of-plane vorticity contours ($\omega_z c/U_\infty$, range ± 40) for $Re = 10,000$. Left panel: present results, right panel: results by Visbal [21] on baseline grids.

Compared to this, the present baseline resolution is finer along the airfoil surface, but coarser in the wall-normal direction. Use of finer resolutions are feasible, however, the simulations on thin, flat airfoil as planned in this study used similar resolutions as in figure 3, in order to facilitate several parametric studies in reasonable time. The verification study for SD7003 airfoil, thus allows estimation of the predictive capability of the solver on grid resolutions comparable to that used for the thin, flat airfoil. The time-step used for the present incompressible flow simulations is also 4-times larger than those used by Visbal [21] in his compressible flow solver.
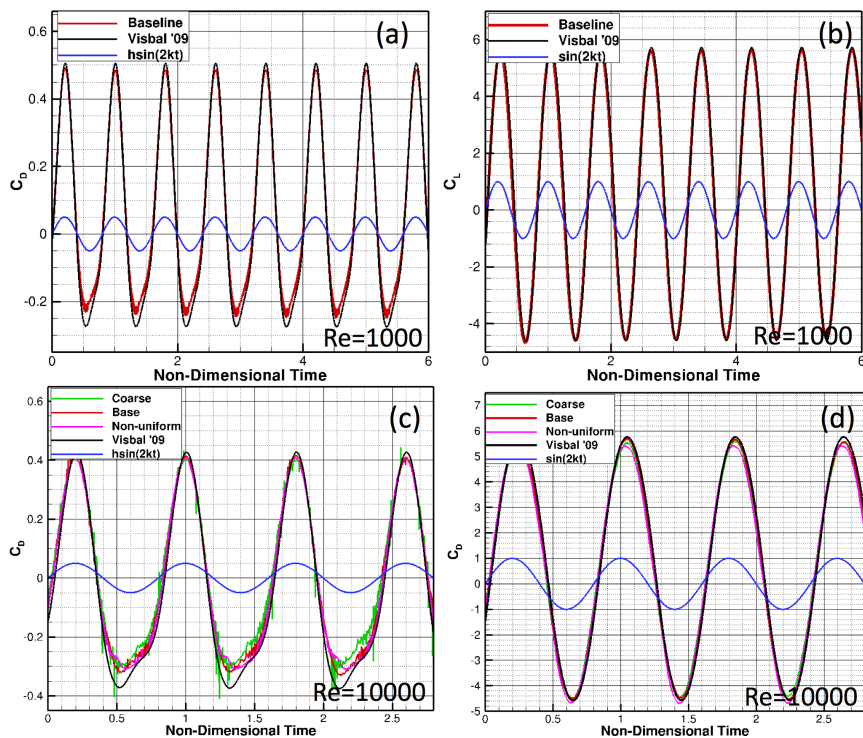

Figure 5: Two-dimensional loads on SD7003 airfoil at two different Reynolds numbers compared with the high-fidelity solver, FDL3DI [21]: (a,b) Drag and lift coefficients at $Re = 1000$, (c,d) drag and lift coefficients at $Re = 10000$. Predictions for baseline, coarse and non-uniform grids are shown.

4

The flow conditions correspond to angle of attack (α) of 4°, non-dimensional plunge amplitude $h_0 = h/c = 0.05$, reduced frequency of plunging motion, $k = \pi f c/U_\infty = 3.93$, where U_∞ is the free-stream velocity. A ramp function was used to allow smooth transition to the periodic plunging motion:

$$h(t) = h_0 \sin[2kF(t)t]; \quad F(t) = 1 - e^{-at}; \quad a = 4.6/t_0; \quad t_0 = 0.5. \tag{1}$$

Figure 4 shows contour plots of out-of-plane vorticity at four different phase angles compared with corresponding plots by Visbal [21] showing very good qualitative comparison of the vortex structures on the baseline grid. Quantitative comparison of the lift and drag coefficients were also obtained for $Re = 10^3, 10^4$ as shown in figure 5. It is seen that, for both Reynolds numbers the loads are well predicted. The drag coefficient is slightly under-predicted for $Re = 10000$, near the phase 3/4 of the periodic cycle. This may be attributed to the coarser wall-normal resolution in the present simulations compared to those by Visbal [21]. However, the asymmetric nature of the drag coefficient (especially for $Re = 10000$) is capture by present simulations. *This asymmetry actually results in mean thrust for these high-frequency plunging cases.* This case study also verifies the predictive capability of the present solver on grids comparable to those used in the thin airfoil study described below.

3.2 Flow Over Thin Flat Airfoil

Flow over a thin, flat airfoil at $Re = 14700$ and an angle of attack (α) of 20° is investigated. The chord length (c) is 20 cm, the thickness to chord ratio is 0.02, and the actuator length to chord ratio is 0.3. The airfoil has elliptical rounded edges with a ratio of 5:1. Grid resolutions used in the present calculations are given in

Grid	$\Delta x/c$	$\Delta y/c$	$\Delta t U_\infty/c$
Baseline	0.00166	0.00166	0.000125
Coarse (Non-Uniform)	0.005	0.00166	0.00025

Figure 6: Cartesian grid resolution for thin, flat airfoil studies.

figure 6. The baseline resolution is finer than that used for corresponding studies on the plunging SD7003 as discussed earlier. The effect of leading edge actuation is studied in two-steps: (i) static actuation and (ii) dynamic actuation.

As the first step, effect of the *static actuation* of the leading edge on the flowfield is investigated. The actuation angle (θ) (measured anti-clockwise from the axis of the airfoil) is set to 20°, giving an effective angle of attack of $\alpha_{\text{eff}} = 13.77°$. This static actuation provides an effective camber to the airfoil and is expected to reduce flow separation and drag. Effect on the lift coefficient and mean lift-to-drag ratio are investigated. As the second step, sinusoidal oscillation of the leading edge actuator at different frequencies (1, 3, 5, 10, and 20 Hz), corresponding to the reduced frequencies of $k = \pi f c/U_\infty = 0.57, 1.71, 2.86, 5.71,$ and 11.4, respectively. The actuation amplitudes are varied over range of ($\Delta\theta = 2.5°, 5°,$ and 10°). These vary the effective angles of attack over a wide range: $\alpha_{\text{eff}} = 12.92 - 14.6°, 12.04 - 15.4°$ and $10.2 - 17°$, respectively. The oscillatory actuations are about the mean actuator angle of $\theta = 20°$.
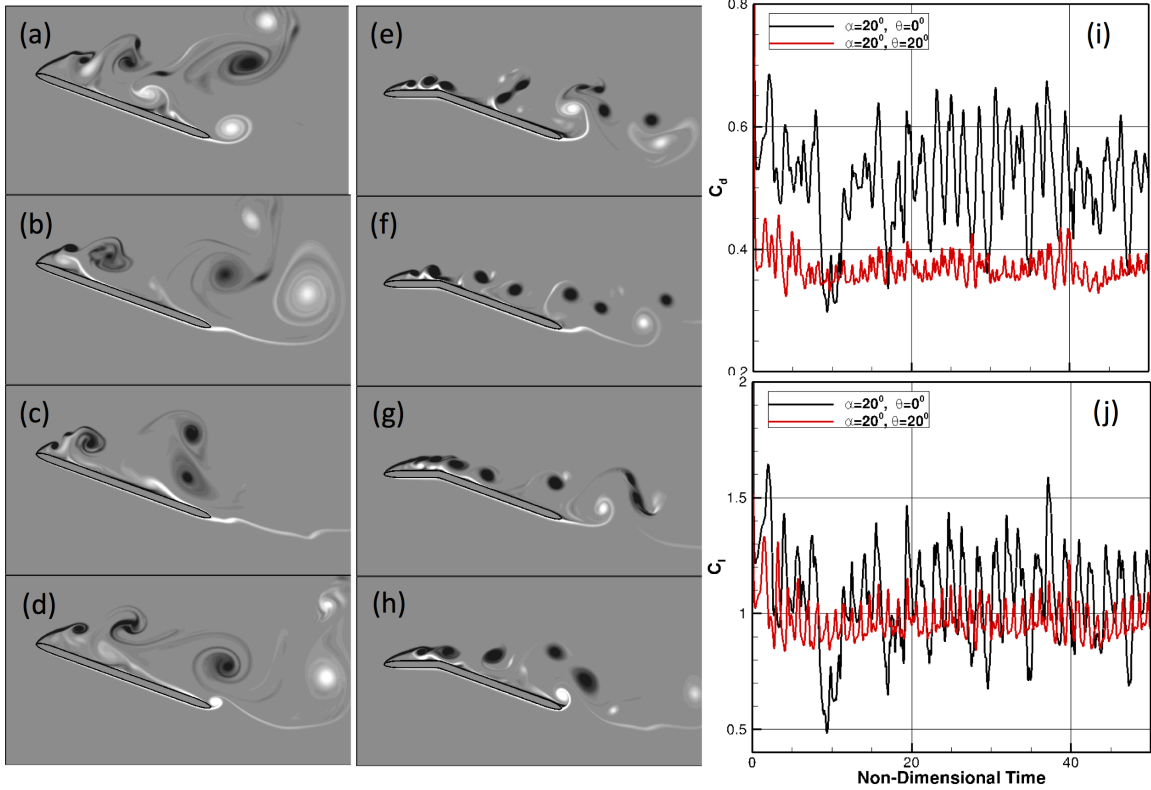
5

Figure 7: Effect of static actuation of the leading edge on flow structure as well as lift and drag for $\alpha = 20°$, $Re = 14700$: (a-d) out-of-plane vorticity contours ($\omega_z c/U_\infty = \pm 60$) for $\theta = 0°$, (e-h) out-of-plane vorticity for $\theta = 20°$ (snapshots are $tU_\infty/c = 2.06$ apart), (i) temporal evolution of drag coefficient for $\theta = 0, 20°$, (j) temporal evolution of lift coefficient for $\theta = 0, 20°$.

The effect of static actuation of the leading edge, with $\theta = 20°$ for an angle of attack (α) of $20°$, was first investigated (see figure 7). For no actuation, the lift and drag coefficients vary significantly for this high angle of attack, showing fluctuations due to passage of vortical structures pas the leading edge. The flow is highly separated with a large wake region. With simple static actuation, the magnitude of the mean drag coefficient is reduced (from 0.502 without actuation to 0.369 with actuation), whereas the mean lift coefficient is not altered significantly (from 1.03 without actuation to 0.97 with actuation). Also with actuation, the range over which the lift and drag coefficients oscillate are reduced significantly. The mean lift-to-drag ratio is increased from 2.06 (without actuation) to 2.63 (with actuation), a 27.67% increase. These results are obtained on the baseline grid, with similar levels of increase in mean lift-to-drag
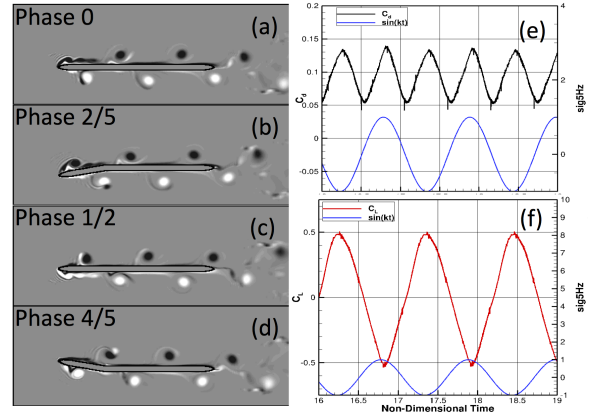

Figure 8: Effect of dynamic actuation of the leading edge on flow structure as well as lift and drag for $\alpha = 0°$, $Re = 14700$: (a-d) out-of-plane vorticity contours ($\omega_z c/U_\infty = \pm 60$) for $\Delta\theta = \pm 10°$ at 10 Hz, (e) temporal evolution of drag coefficient, (f) temporal evolution of lift coefficient.
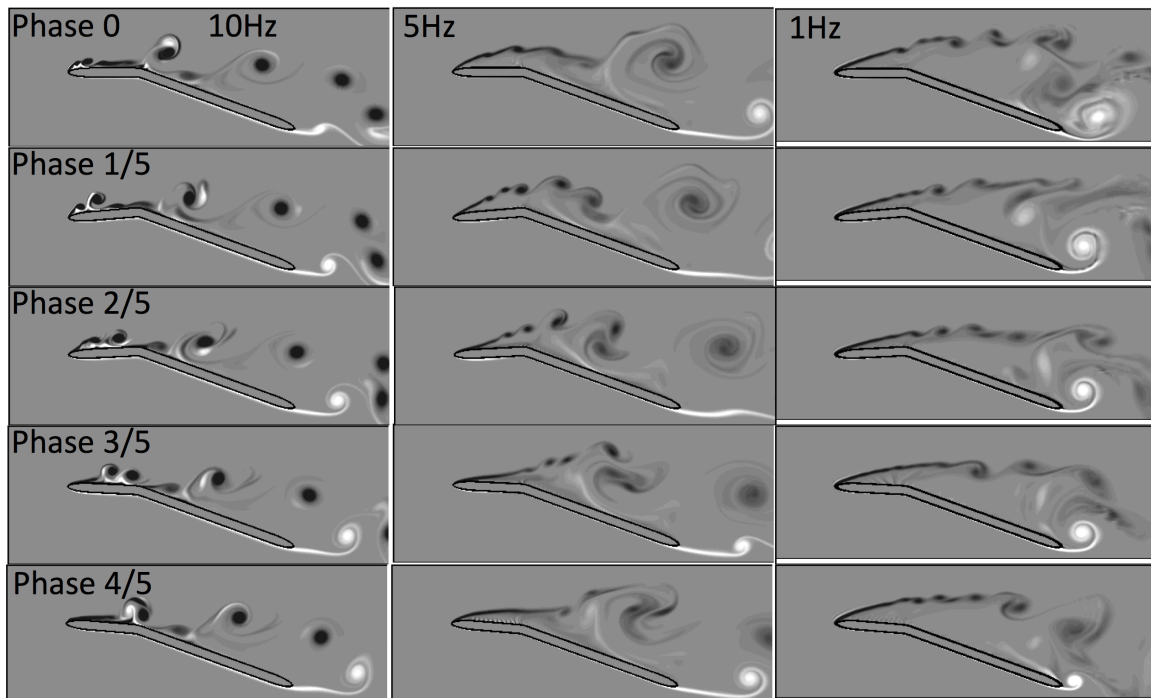
ratio shown by the coarse grid.

Figure 9: Out-of-plane vorticity contours ($\omega_z c/U_\infty = \pm 60$) showing effect of dynamic actuation of the leading edge ($\Delta\theta = \pm 5°$) on flow structure for $\alpha = 20°$, $Re = 14700$. Left panel: 10 Hz ($k = 5.71$), middle panel: 5 Hz ($k = 2.86$), right panel: 1 Hz ($k = 0.57$) showing different phases of the actuation cycle.

High frequency, periodic plunging applied to entire airfoil can result in a *net thrust* [21], for example the case of SD7003 airfoil discussed earlier leads to a net mean thrust. In order to investigate if the present leading edge actuation also provides a thrust component, simulations were performed at 0° angle of attack with the leading edge actuated to undergo sinusoidal oscillations around the mean position at different frequencies and amplitudes. Figure 8 shows the flow structure and evolution of the out-of-plane vorticity at different phase angles for an actuation at 10 Hz and amplitude of 10° at $Re = 14700$. Also shown is the temporal history of drag and lift coefficients over a few cycles. It is observed from the vorticity contours that the oscillatory actuation creates periodic vorticies which pass along the airfoil resulting in oscillatory variations in lift and drag coefficients. For the actuator length to chord ratio of 30%, it was found that the sinusoidal actuation resulted in a small net mean thrust and also a positive mean lift. This study shows that the present actuation does not result in a mean thrust. A longer actuator may be necessary to obtain thrust; however, as shown later, this simple actuation can indeed provide increased mean lift-to-drag ratio at higher angles of attack.

The effect of dynamic actuation of the leading edge on the flow structure and drag/lift characteristics was investigated by oscillating the leading edge around a mean angle of $\theta = 20°$. Various frequencies (20,10, 5, 3, and 1 Hz) and amplitudes (10°, 5°, and 2.5°) were investigated. Figure 9 shows the flow structure over one
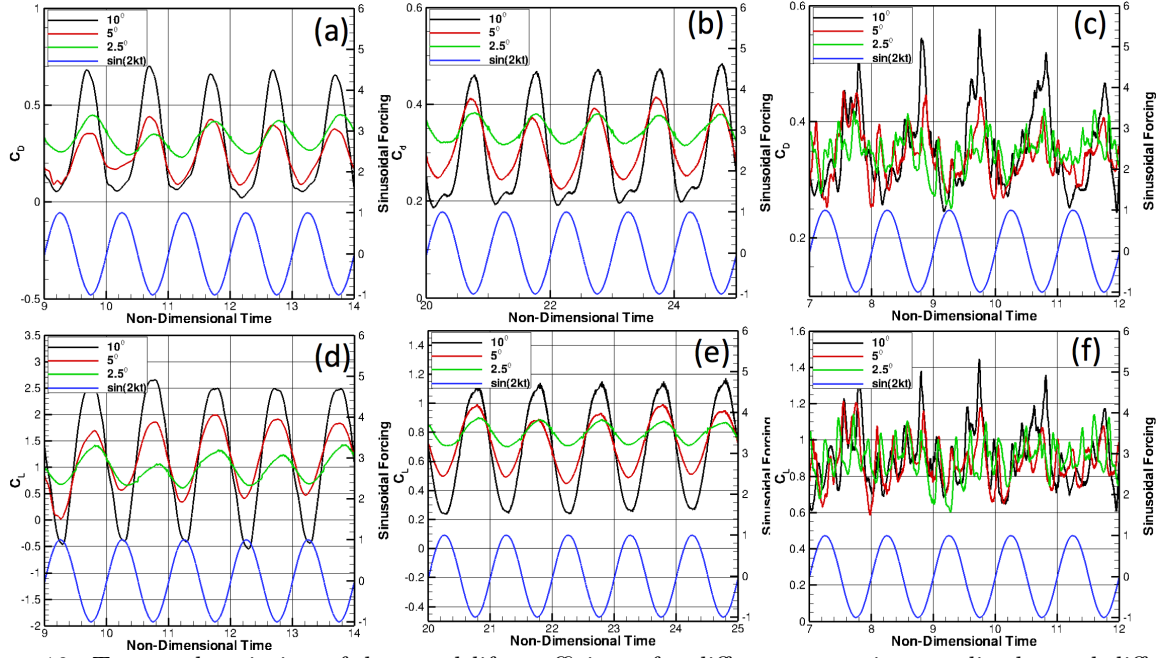
Figure 10: Temporal variation of drag and lift coefficients for different actuation amplitudes and different frequencies: (a) C_d at 10 Hz, (b) C_d at 5 Hz, (c) C_d at 1 Hz, (d) C_l at 10 Hz, (e) C_l at 5 Hz, (f) C_l at 1 Hz.

cycle of actuation for an amplitude of $\Delta\theta = \pm5°$ at three different frequencies. It is seen that for the high frequency of 10 Hz ($k = 5.71$), strong vortical structures created near the leading edge travel downstream. Vortex pairing mechanisms are observed with the vortices remaining close to the airfoil surface resulting in a smaller wake region. For lower frequencies (5 and 1 Hz), the separated flow near the leading edge and the shear layer oscillate with the actuator motion. The flow remains separated over most of the cycle giving a larger wake, and the breakdown of vortices observed in the high-frequency case is absent.

Figure 10 shows the temporal variations of lift and drag coefficients for different frequencies and actuation amplitudes over a range of cycles. It is observed that for frequencies of 10 and 5 Hz, the lift/drag coefficients are periodic with a phase difference compared to the actuator motion. For large amplitude actuations (10°), the variations in lift and drag around a mean are also large. For lower frequencies of 1 Hz and also 3 Hz (not shown), the drag and lift coefficients oscillate, however, several periods appear superimposed. The fluctuations show similar characteristics as the static-actuation, especially for low frequency and low amplitude oscillations.

Tables 1–3 summarize the effect of static and dynamic actuation of the leading edge on the mean lift and drag coefficients for different actuation frequencies and amplitudes. Also compared are the mean lift-to-drag ratios to that obtained with no actuation. It is observed that any actuation (static or dynamic) results in an increase of mean lift-to-drag ratio compared to no actuation. With static actuation (i.e. $\theta = 20°$ for $\alpha = 20°$), an increase of 27.7% was observed. As shown in figure 7, the temporal variation of the lift and drag coefficients have a range of frequencies superimposed.

8

Table 1: $\bar{C}_d$ and $\bar{C}_l$ for $Re_C = 14700$, $\Delta\theta = 10°$.

α_0	θ	frequency (reduced)	$\bar{C}_d$	$\bar{C}_l$	$\bar{C}_l/\bar{C}_d$	% increase
20°	0°	0	0.502	1.034	2.06	-
20°	20°	0	0.369	0.97	2.63	27.7%
20°	20°	10 Hz (5.71)	0.281	1.11	3.96	91.75%
20°	20°	5 Hz (2.86)	0.32	0.75	2.35	13.75%
20°	20°	1 Hz (0.571)	0.34	0.85	2.5	21.3%

Table 2: $\bar{C}_d$ and $\bar{C}_l$ for $Re = 14700$, $\Delta\theta = 5°$.

α_0	θ	frequency (reduced)	$\bar{C}_d$	$\bar{C}_l$	$\bar{C}_l/\bar{C}_d$	% increase
20°	20°	20 Hz (11.42)	0.36	1.06	2.94	43%
20°	20°	10 Hz (5.71)	0.224	1.12	5	142%
20°	20°	5 Hz (2.86)	0.31	0.76	2.45	19%
20°	20°	1 Hz (0.571)	0.34	0.89	2.61	22.78%

Table 3: $\bar{C}_d$ and $\bar{C}_l$ for $Re = 14700$, $\Delta\theta = 2.5°$.

α_0	θ	frequency (reduced)	$\bar{C}_d$	$\bar{C}_l$	$\bar{C}_l/\bar{C}_d$	% increase
20°	20°	20 Hz (11.42)	0.3066	1.025	3.34	62.2%
20°	20°	10 Hz (5.71)	0.30	0.934	3.11	51.1%
20°	20°	5 Hz (2.86)	0.35	0.795	2.27	10.26%

With dynamic actuation at high frequencies (10 and 20 Hz) further increase in mean lift-to-drag ratios were observed. Specifically, for actuation amplitudes of $\Delta\theta = \pm5°$ and $\pm2.5°$ at high frequencies, an increase in mean lift-to-drag ratio of more than 50% was observed. In addition, for dynamic actuation, the temporal behavior of the lift and drag coefficients are periodic and predictable corresponding to the actuation frequency. With higher amplitudes of actuator motion, the range over which the lift and drag coefficients varied also increased. For lower frequencies (1, 3 and 5 Hz), the increase in mean lift-to-drag ratio is lower and the temporal variation in drag and lift coefficients show multiple frequencies superimposed similar to that observed in static actuation. These results suggest that high frequency actuation of the leading edge (either as designed or flow-induced) provide strong potential for development of control strategies. Specifically, these effects need to be investigated for airfoils undergoing transient maneuvers such as pitching or heaving.

4   Summary and Future Work

Effect of oscillatory actuation of the leading edge of a thin, flat, rigid airfoil on MAV performance was investigated using two-dimensional simulations at low Reynolds number (14700) and 20° angle of attack. A second-order accurate, fictitious domain method was used for this moving boundary problem on a fixed background mesh. The numerical method was thoroughly verified for its accuracy and predictive capability on canonical problems of flow over a cylinder and sphere at different Reynolds numbers, flow over a NACA hydrofoil, flow generated by an inline oscillation of the cylinder and flow over a plunging SD7003 airfoil. Reasonable comparison was obtained for plunging studies of SD7003 airfoil compared to AFRLs high-fidelity

solver FDL3D for Reynolds numbers of 10^3 and 10^4.

Flow over a thin, flat airfoil at high angle of attack was study with and without actuation of the leading edge. Leading edge actuation involving rotation around a hinge located at 30% chord length can be used to reduce the effective angle of attack without significantly reducing the lift. Reduction in effective angle of attack and the added camber, results in reduced drag. A 27% increase in mean lift-to-drag ratio was observed for static actuation cases, wherein the leading edge flap was horizontal ($\theta = 20°$). Actuated leading edge at different reduced frequencies (0.57-11.42) and amplitudes (2.5° -10°) were also studied. It was observed that high frequency actuation of $10, 20$ Hz ($k = 5.71, 11.42$), further increases the mean lift-to-drag ratio ($> 50\%$). It also provides predictable pattern of lift and drag variations. Further analysis to study effect on mean flow/pressure, accounting for three-dimensional, transition effects as well as experimental data are needed to corroborate these findings.

The present work indicated that the leading edge actuation using a hinged flap provides a means to directly influence the leading edge stall condition and unsteady lift behavior while not adding complexities associated with blowing or suction that may not be practical, for small wings with weight constraints. Control strategies based on the present leading edge actuation are of direct relevance to small-size MAVs undergoing maneuvers and are pragmatic as designing simple piezo-based actuators is straightforward. The present simple modification to the wing configuration also facilitates development of actuators and controllers for airfoils with considerable size and weight restrictions. For instance, typical characteristic lengths for MAV are in the range of 8–15 cm, with operating speeds on the order of 50 km/h. Improving the flight performance of these vehicles can enhance surveillance, search and rescue, and sensor mobility, while yielding vehicles that are more disposable.

Although this work investigated rigid airfoils, the results are of direct relevance to other forms of leading edge flow control which are more amenable to small scale MAV implementation of current interest to AFOSR; for example, surface deformations via piezo-electric actuators or aero-elastically tailored structures. In addition, concepts of passive control, with spring mounted hinge are also feasible leading to flow-induced actuation of the leading edge.

The summer research at AFRL's computational sciences division has resulted in several opportunities for future collaborations with AFRL scientists and researchers. At Oregon State, new projects for senior students are initiated to build and modify the existing physical setup and measure lift and drag coefficients. A University Honors College thesis [27] has also been completed and couple of students, supported as Teaching Assistants, are working toward their Master's degree on related topics. This research work will be presented at American Physical Society's Division of Fluid Dynamics Meeting in Los Angeles in November.

References

[1] Y. Hoarau, M. Braza, Y. Ventikos, D. Faghani, G. Tzabiras, Organized modes and the three dimensional transition to turbulence in the incompressible flow around a NACA0012 wing, J. Fluid Mech. 496 (2003) 63–72.

[2] H. Nishimura, Y. Taniike, Aerodynamic characteristics of fluctuating forces on a circular cylinder, J. Wind Eng., Ind. Aerodynamics 89 (2001) 713–723.

[3] C. Sicot, S. Auburn, S. Loyer, P. Devinant, Unsteady characteristics of the static stall of an airfoil sujected to freestream turbulence level up to 16%, Exp. in Fluids 41 (2006) 641–648.

[4] A. Fabula, This airfoil theory applied to hydrofoils with a single finite cavity and arbitrary free-streamline detatchment, J. Fluid Mech. 12 (1962) 227–240.

[5] H. Kao, Some aspects of airfoil stall in low speed flow, J. Aircraft 11 (3) (1974) 177–180.

[6] S. Brunton, C. Rowley, K. Taira, T. Colonius, J. Collins, D. Williams, Unsteady aerodynamic forces on small-scale wings: experiments, simulations and models, in: 46 th AIAA Aerospace Sciences Meeting and Exhibit, American Institute of Aeronautics and Astronautics, 1801 Alexander Bell Drive, Suite 500, Reston, VA, 20191-4344, USA,, 2008.

[7] W. Geissler, H. Sobieczky, H. Vollmers, Numerical study of the unsteady flow on a pitching airfoil with oscillating flap, in: European Rotorcraft Forum, 24 th, Marseilles, France, 1998.

[8] Y. Lu, G. Shen, G. Lai, Dual leading-edge vortices on flapping wings, Journal of Experimental Biology 209 (24) (2006) 5005.

[9] F. Muijres, L. Johansson, R. Barfield, M. Wolf, G. Spedding, A. Hedenstrom, Leading-edge vortex improves lift in slow-flying bats, Science 319 (5867) (2008) 1250.

[10] M. Dickinson, F. Lehmann, S. Sane, Wing rotation and the aerodynamic basis of insect flight, Science 284 (5422) (1999) 1954.

[11] K. Taira, W. Dickson, T. Colonius, M. Dickinson, C. Rowley, Unsteadiness in flow over a flat plate at angle-of-attack at low Reynolds numbers, in: 45 th Aerospace Sciences Meeting and Exhibit, AIAA,(AIAA 2007-710).

[12] K. Taira, T. Colonius, Three-dimensional flows around low-aspect-ratio flat-plate wings at low Reynolds numbers, Journal of Fluid Mechanics 623.

[13] T. Colonius, C. Rowley, G. Tadmor, D. Williams, K. Taira, W. Dickson, M. Gharib, M. Dickinson, Closed-loop control of leading-edge and tip vortices for small UAV, in: Conference on Active Flow Control, 2006.

[14] T. Mueller, J. DeLaurier, An overview of micro air vehicle aerodynamics.' Fixed and flapping wing aerodynamics for micro air vehicle applications, Progress in Astronautics and Aeronautics 195 (2001) 1–10.

[15] A. Pelletier, T. Mueller, Low Reynolds number aerodynamics of low-aspect ratio, thin/flat/cambered-plate wings, J. of Aircraft 37 (5) (2000) 825–832.

[16] A. Broeren, M. Bragg, Unsteady stalling characteristics of thin airfoils at low Reynolds numbers. Fixed and flapping wing aerodynamics for micro air vehicle applications, Progress in Astronautics and Aeronautics 195 (2001) 191–213.

[17] S. Yarusevych, P. Sullivan, J. Kawall, Airfoil boundary layer separation and control at low Reynolds numbers, Exp. Fluids 38 (2005) 545–547.

[18] M. Fuchiwaka, K. Tanaka, M. Nakashima, Characteristics of dynamic thrust on an unsteady airfoil in pitching and heaving motions, FEDSM2007-37222, Proc. FEDSM20007, Joint ASME/JSME Fluids Engineering Conf., San Diego, CA.

[19] S. Apte, M. Martin, N. Patankar, A numerical method for fully resolved simulation (FRS) of rigid particle-flow interactions in complex flows, Journal of Computational Physics (2008) doi:10.1016/j.jcp.2008.11.034.

[20] M. Visbal, High-fidelity simulation of transitional flows past a plunging airfoil, AIAA paper 391 (2009) 2009.

[21] M. Visbal, R. Gordnier, M. Galbraith, High-fidelity simulations of moving and flexible airfoils at low Reynolds numbers, Experiments in Fluids 46 (5) (2009) 903–922.

[22] S. Apte, N. Patankar, A numerical scheme for fully resolved direct numerical simulation of arbitrary shaped rigid particles in turbulent flows, J. Comp. Phy. (to be submitted).

[23] S. Apte, J. Finn, A variable density fictitious domain method for fully resolved simulation of high-density ratio fluid-particle systems, in: ICMF2010, Seventh International Conference on Multiphase Flow, Tampa Bay, FL.

[24] S. Apte, N. Patankar, A formulation for fully resolved simulation (FRS) of particle–turbulence inter-
actions in two-phase flows, International Journal of Numerical Analysis and Modeling 5, Suppl (2008)
1–16.

[25] P. Moin, S. Apte, Large eddy simulation of multiphase reacting flows in complex combustors, AIAA J.
(special issue on 'Combustion Modeling and LES: Development and Validation Needs for Gas Turbine
Combustors) 44 (2006) 698–710.

[26] G. McGowan, A. Gopalarathnam, M. Ol, J. Edwards, D. Fredberg, Computation vs. experiment for
high-frequency low-reynolds number airfoil pitch and plunge, AIAA 653 (2008) 2008.

[27] K. Drost, Direct Numerical Simulation of a Flat Wing with a Movable Front Flap at High Angles of
Attack and Low Reynolds Numbers, University Honors College B.S. Thesis, Oregon State University.